doi:10.1006/jmbi.2001.4469 available online at http://www.idealibrary.com on IDEAL® J. Mol. Biol. (2001) 307, 637–656

JMB

Thermodynamics of Trimer-of-Hairpins Formation by the SIV gp41 Envelope Protein

Ilian Jelesarov[1]* and Min Lu[2]*

[1]*Biochemisches Institut der Universität Zürich Winterthurerstrasse 190 CH-8057, Zürich, Switzerland*

[2]*Department of Biochemistry Weill Medical College of Cornell University, New York NY 10021, USA*

**Corresponding authors*

The gp41 envelope protein mediates the entry of primate immunodeficiency viruses into target cells by promoting the fusion of viral and cellular membranes. The structure of the gp41 ectodomain core represents a trimer of identical helical hairpins in which a central trimeric coiled-coil made up of three amino-terminal helices is wrapped in an outer layer of three antiparallel carboxyl-terminal helices. Triggering formation of this fusion-active gp41 conformation appears to cause close membrane apposition and thus overcome the activation energy barrier for lipid bilayer fusion. We present a detailed description of the folding thermodynamics of the simian immunodeficiency virus (SIV) gp41 core by using a recombinant trimeric N34(L6)C28 model. Differential scanning calorimetry and spectroscopic experiments on denaturant-induced and thermal unfolding indicate that the free energy of association of three 68 residue N34(L6)C28 peptides to a trimer-of-hairpins is 76 kJ mol^{-1} at pH 7.0 and 25 °C in physiological buffer. The associated enthalpy change, ΔH_{unf}, is 177 kJ mol^{-1}, while the entropy of unfolding, ΔS_{unf}, is 0.32 kJ K^{-1} mol^{-1}. The temperature of maximal stability is close to 20 °C. The unfolding heat capacity increment is ~9 kJ K^{-1} mol^{-1} (~45 J K^{-1} mol $residue^{-1}$), which is lower than expected for unfolding of the trimer to an extended and fully hydrated polypeptide chain. Replacement by isoleucine of the polar residues Thr582 or Thr586 buried in the N-terminal trimeric coiled-coil interface leads to very strong stabilization of the trimer-of-hairpins, 30-35 kJ mol^{-1}. Single-point mutations in the central coiled-coil thus strongly stabilize the gp41 core structure. These thermodynamic characteristics may be important for the refolding of the gp41 envelope protein into its fusion-active conformation during membrane fusion.

Keywords: gp41; trimer-of-hairpins; envelope glycoprotein; membrane fusion; coiled-coil

Introduction

Infection of cells by primate immunodeficiency viruses (human, HIV; simian, SIV) requires fusion of the viral and cellular membranes, a process mediated by the trimeric envelope glycoprotein complex on the surface of the virion. This envelope protein is initially synthesized as the precursor gp160, which is proteolytically cleaved into two non-covalently associated subunits, gp120 and

Abbreviations used: DSC, differential scanning calorimetry: K_{unf}, unfolding equilibrium constant; ΔG_{unf}, unfolding free energy; ΔH_{unf}, unfolding enthalpy; ΔS_{unf}, unfolding entropy; ΔC_p^{unf}, unfolding heat capacity; HIV-1, human immunodeficiency virus type 1; SIV, simian immunodeficiency virus; GdmCl, guanidinium hydrochloride; m_D, the first derivative of the observed unfolding free energy in respect to the denaturant concentration, units of kJ mol^{-1} M^{-1}; [D], denaturant concentration; $[D]_{1/2}$, denaturant concentration at the mid-point of isothermal denaturant-induced transition; $[\theta]_{222}$, molar ellipticity per residue at 222 nm; T_m, midpoint of thermal unfolding; *ASA*, solvent-accessible surface; ΔASA_{ap}, change of accessible apolar surface upon unfolding (in Å^2); ΔASA_{ar}, change of accessible aromatic surface upon unfolding (in Å^2); ΔASA_{pol}, change of accessible plolar surface upon unfolding (in Å^2); a_x, unfolding heat capacity increment normalized per Å^2 in units of J $K^{-1}mol^{-1}$ Å^{-2}, x=ap, ar or pol, denoting apolar, aromatic or polar surface, respectively; ΔG(W), unfolding free energy in aqueous buffer; ΔG(D), unfolding free energy in the presence of denaturants.

E-mail addresses of the corresponding authors: iljel@bioc.unizh.ch; mlu@mail.med.cornell.edu

0022-2836/01/020637–20 $35.00/0

gp41.[1,2] Upon binding of gp120 to the CD4 glycoprotein and a chemokine receptor on the T-cell surface, gp41 undergoes conformational changes that promote membrane fusion between virus and target cell during infection, as well as between infected cells and uninfected cells during multinucleated giant cell (syncytium) formation.[3,4] By analogy with the acidic pH-induced structural changes in the hemagglutinin (HA) protein of influenza virus, the gp41-mediated viral entry process is postulated to involve a structural rearrangement and refolding in the envelope protein complex from a metastable native (prefusogenic) state to a stable fusion-active (fusogenic) conformation.[5–8] This receptor binding-triggered gp41 activation is an obligate step in virus entry into target cells, and inhibitors of this process are now in clinical or preclinical development.[9–12]

The extracellular ectodomain of the gp41 envelope protein contains several characteristic features that may be important for formation of its fusogenic conformation during activation of retroviral membrane fusion. First, it has a hydrophobic, glycine-rich sequence, referred to as the fusion peptide, at the N terminus and this is thought to insert into the cellular membrane at an early step of the fusion process.[13,14] Second, there are two regions with a 4,3 hydrophobic (heptad) repeat predicted to form coiled-coil structures.[15–17] The N-terminal heptad-repeat region is immediately C-terminal to the fusion peptide, while the C-terminal heptad-repeat region is located adjacent to the viral membrane (see Figure 1(a)). Between these two heptad-repeat regions is a loop region containing two cysteine residues. Biophysical studies demonstrated that two peptides (termed N and C peptides) corresponding to these two heptad-repeat regions associate to form a stable, α-helical trimer of antiparallel heterodimers.[18–20] Analysis of this trimer-of-hairpins structure by X-ray crystallography and NMR shows that three N helices form a central three-stranded coiled-coil, whereas three C helices pack in the reverse direction into highly conserved hydrophobic grooves around the outside of this coiled-coil.[21–26] This structure likely represents the fusion-active state of gp41, and shares features with the fusion pH-induced conformation of influenza virus HA.[5,19,22] This proposition is supported by the observation that a monoclonal antibody specifically recognizing the helical-hairpin structure binds to the surface of HIV-1-infected cells only after interaction of the envelope protein complex with soluble CD4.[27]

Based upon a wealth of biochemical and structural data, the following model of gp41-mediated membrane fusion has been proposed.[4] Initially, gp41 exists in a prefusogenic conformation within the trimeric envelope glycoprotein spike. Binding of gp120/gp41 to CD4 induces initial conformational changes in gp120 that expose the co-receptor binding site, and the subsequent binding of gp120 to the co-receptor initiates the membrane fusion process itself.[3,28,29] Next, a transient gp41 species or the so-called pre-hairpin intermediate is formed by exposure of the fusion-peptide region and concurrent formation of the N-terminal coiled-coil trimer.[30–32] The association of the C-terminal heptad-repeat region with the N-terminal coiled-coil resolves the prehairpin intermediate into the fusion-active hairpin structure and thus leads to the local apposition of viral and cellular membranes.[25,30,33] This model implies that energy made available from the trimer-of-hairpins formation is harnessed to break the energy barrier for fusion of two lipid bilayers, which is energetically unfavorable. It would appear that the refolding of gp41 into its fusogenic conformation and the process of membrane apposition and fusion are mechanistically coupled and thermodynamically linked. Thus, the conformational stability of the trimer-of-hairpins structure may play a critical role in driving membrane fusion and a better understanding of the thermodynamics of trimer formation is therefore required. However, thermodynamic studies of the HIV-1 gp41 ectodomain core have been hampered by its tendency towards irreversible denaturation and aggregation, and the use of differential scanning calorimetry (DSC) or spectroscopy has been useful only as a qualitative guide to stability. We now have constructed a recombinant model of the SIV gp41 core that exhibits a well-defined two-state transition between folded trimer and unfolded monomer, allowing us to analyze for the first time the folding thermodynamics of the trimer-of-hairpins structure and two strongly stabilizing coiled-coil mutants.

The conformational stability of multimeric proteins has been described quantitatively in only about a dozen cases as compared to the wealth of thermodynamic data available on monomeric folding units.[34–47] Even fewer studies have addressed the sensitivity of such proteins on mutations.[37,48–50] Folding of protein multimers, especially when tightly coupled to association of intrinsically unstable monomers, requires special attention. Stabilization energy is gained from inter-subunit interactions, and folding is accompanied by reduction of rotational and translational entropy.[51–53] Understanding the balance between energetic factors driving multimer folding is, however, not only of theoretical interest. Conformational equilibria are concentration-dependent and knowledge of this dependency as a function of environmental parameters might provide clues about the population of functional multimers in the living cell, where protein levels are rarely as high as in a biophysical experiment. Interestingly, the coupling of the monomer-trimer equilibrium of the gp41 ectodomain to its folding is thought to play a critical role in the biology of HIV-1 entry and its inhibition.[54]

Results

Design of SIV N34(L6)C28

The ectodomain core of the HIV-1 gp41 denatures irreversibly with temperature and forms an insoluble aggregate under physiological conditions, and so the T_m measured by circular dichroism spectroscopy (CD) cannot be used to analyze the conformational stability of the fusion-active hairpin structure in a quantitative way.[19] Previous studies showed that heat denaturation of the SIV trimeric N36(L6)C34 complex at peptide concentrations below ~20 μM proceeds with a cooperative two-state folding-unfolding transition.[55] To study the thermodynamics of trimer-of-hairpins denaturation over a broad range of peptide concentration, we constructed a recombinant model for the SIV gp41 ectodomain. This model, named N34(L6)C28, consists of the shortened N34 and C28 peptides that are connected by a six residue flexible linker in place of the disulfide-bonded loop region (Figure 1(a)). In addition, we have prepared two mutants that strongly stabilize the fusion-active conformation of gp41 by replacing with isoleucine either Thr582 (in a heptad ***d*** position) or Thr586 (in a heptad ***a*** position) of the N-terminal trimeric coiled-coil. These mutant peptides were named T582I and T586I, respectively.

In CD measurements performed at neutral pH, 10 μM N34(L6)C28, T582I, and T586I are fully folded and melt cooperatively and reversibly. Sedimentation equilibrium measurements indicate that each peptide sediments as a trimer over a tenfold range of protein concentration (10 to 100 μM) (Figure 2). The X-ray crystal structures of the N34(L6)C28 and T586I peptides were determined at 3.1 and 2.48 Å resolution, respectively (K. Tan, A. Mosyak, J. Liu, H. Ji, M. L. & J. H. Wang, unpublished results). The overall structures of N34(L6)C28 and T586I are very similar to the analogous structure in HIV-1 gp41. In each case, the N34 helices form a parallel three-stranded coiled-coil in the characteristic acute ''knobs-into-holes'' arrangement. Three C28 helices pack in an antiparallel orientation into three hydrophobic grooves on the surface of the central coiled-coil trimer (Figure 1(b)). Thus, N34(L6)C28, T582I, and T586I form well-structured trimer-of-hairpins structures.

Thermal unfolding followed by CD

The CD spectra of the three peptides show a typical loss of α-helical content when the temperature is raised. Reversibility of thermal unfolding is >95 % at all concentrations and solvent conditions tested (Tables 1, 2, and 3) as assessed from cooling to the starting temperature and repeated heating scans of the same sample. Figure 3(a) shows examples of CD unfolding curves. Before the unfolding transition, the molar ellipticity is the same for all three proteins and increases linearly with temperature. The steepness of the main transition is very similar for N34(L6)C28, T582I, and T586I, indicating that the Thr-to-Ile mutation does not detectably alter the unfolding mechanism. The midpoints of thermal denaturation of the mutant proteins are significantly higher, indicating appreciable stabilization (Figure 3(a)).

Increasing the peptide concentration shifts the transition midpoint to higher temperature, as expected for a system undergoing unfolding from an oligomeric folded state to a monomeric denatured state. Figure 4 illustrates the concen-

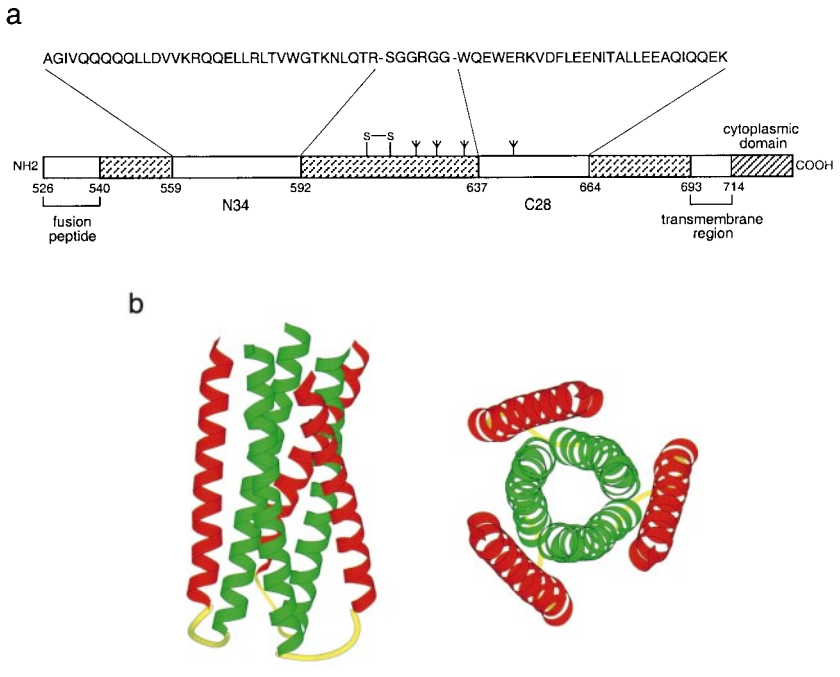

Figure 1. The gp41 ectodomain core. (a) A representation of gp41. The important features of the gp41 ectodomain and the amino acid sequences of the N34 and C28 peptides are shown. N34(L6)C28 consists of N34 and C28 plus a linker of six hydrophilic residues. The disulfide bond and four potential N-glycosylation sites are depicted. The residues are numbered according to their position in SIV gp160. (b) The N34(L6)C28 crystal structure of the HIV-1 gp41 ectodomain core.[24] The left panel shows a side-view of the N34(L6)C28 trimer. The right panel shows an end-on view looking down the 3-fold axis of the trimer. The C28 helices (red) pack against the surface of the trimeric N34 coiled-coil (green). This Figure was created with the program MOLSCRIPT.[95]

Table 1. Thermodynamic parameters from thermal unfolding of N34(L6)C28 measured by circular dichroism and differential scanning calorimetry

	CD		DSC						
Concentration[a] (μM)	T_m[b]	ΔH_m[c]	T_{max}[d] (K)	ΔH_{cal}[e]	ΔH_{vH}[f]	ΔH_{mean}[g]	$T_{0.5}$[h]	ΔH_{fit}[i]	$\Delta H_{vH}/\Delta H_{cal}$
4.9	317.7	335							
9.4	321	366							
17.5			325.7	390	428	415	324.1	426	1.09
18.5	325.4	373							
34	327.4	386							
46.8			329.6	416	444	434	328.6	468	1.07
49.3	329.1	400							
53.1[j]			330.2	400	435	428	329.3	415	1.09
55.9	329.3	405							

All values are per mol of trimer; experiments were done in PBS; ΔH values are in kJ mol^{-1}; maximal error of $\Delta H \leqslant 10\,\%$; error of transition temperature <1 K.

[a] Total peptide concentration in monomer equivalents.

[b] Temperature of the transition midpoint from CD experiments ($f_M = 0.5$).

[c] Transition enthalpy at T_m.

[d] Temperature of the maximum of the heat capacity trace ($f_M = 0.59$-0.61).

[e] Calorimetric enthalpy calculated by integration of the excess heat capacity peak.

[f] van't Hoff enthalpy calculated according to equation (A10).

[g] Mean weighted enthalpy calculated as $\Delta H_{mean} = 0.65\Delta H_{vH} + 0.35\ \Delta H_{cal}$.

[h] Temperature of the midpoint of heat release.

[i] At $T_{0.5}$; mean from non-linear regressions incorporating the molecularity, n, as a floating or fixed parameter.

[j] Mean from two experiments.

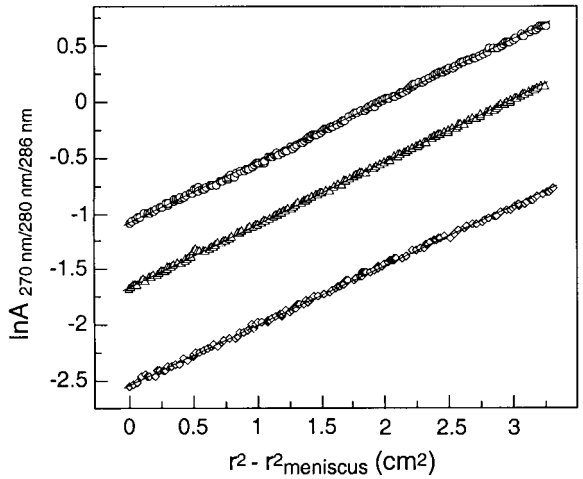

Figure 2. The N34(L6)C28 (open circles), T582I (open triangles), and T586I (open squares) form trimer bundles. Analytical ultracentrifugation data (20,000 rpm) were collected at 20 °C in PBS for N34(L6)C28 (10 μM), T582I (30 μM), and T586I (100 μM). The natural logarithm of the absorbance at 270, 280, or 286 nm is plotted against the square of the radial position. For an ideal single-species system, this plot is linear, with the slope proportional to the molecular mass of the molecule.

tration-dependence of the melting temperature. To increase the range of T_m values, unfolding experiments with T582I and T586I were performed in the presence of small amounts of guanidinium hydrochloride (GdmCl) and urea. Similar experiments with N34(L6)C28 were not possible because of its lower stability in the presence of denaturant. The pre and post-transitional slopes and the shape of the unfolding transition are the same in the presence and in the absence of denaturant, hence the mechanism of thermal unfolding is not changed by addition of denaturant (Figure 4(a)). Values of T_m and ΔH_m are summarized in Tables 1-3.

Thermal unfolding followed by DSC

Figure 3(b) shows examples of DSC scans of N34(L6)C28 and the isoleucine mutants. The excess heat capacity peaks are broad and asymmetric, and the maximum excess molar heat capacity is at temperatures corresponding to 0.59-0.63 of the maximal heat absorption, in agreement with unfolding of a trimer.[56,57] The maximum of the heat capacity trace is concentration-dependent. Unfolding of N34(L6)C28 is reversible up to ~60 μM peptide and of the isoleucine variants up to ~180 μM. Unfolding enthalpies and transition midpoints are insensitive to the scanning rate between 0.5 and 1.5 deg. C min^{-1}. The DSC data are well described by equations (A11) to (A13) (see Appendix) describing a trimer-to-monomer transition. Best fits are obtained for $n = 2.8$-3.2. The

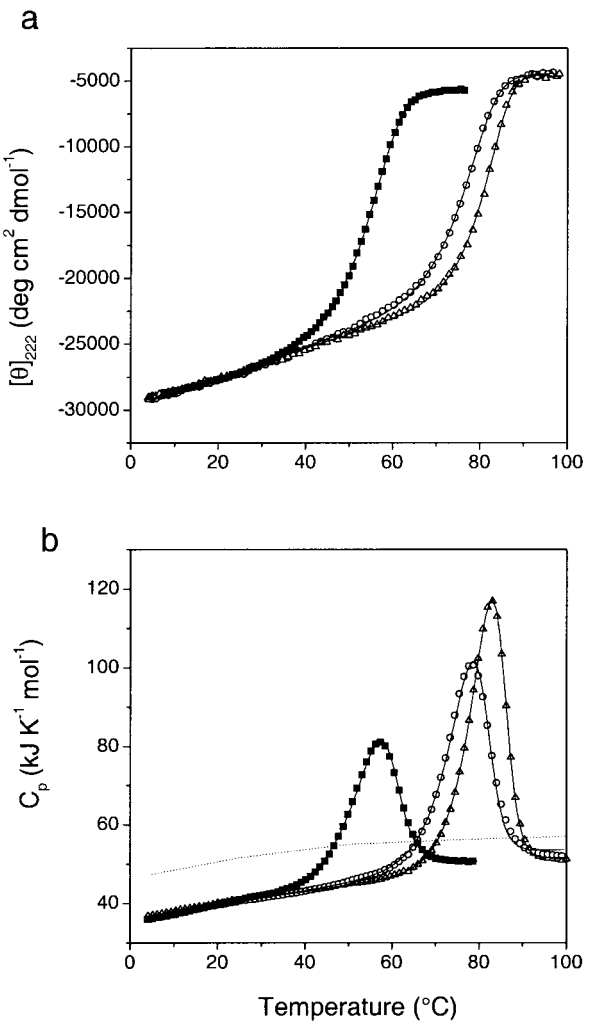

Figure 3. Thermal unfolding monitored by CD and DSC. Melting in PBS and total monomer concentration of 50 μM. Symbols are experimental data collected for N34(L6)C28 (filled squares), T582I (open circles), and T586I (open triangles). (a) Temperature-dependence of the molar ellipticity per residue at 222 nm. Continuous lines are best fits according to equations (A1)-(A4) describing two-state unfolding. (b) Partial molar heat capacity traces recorded at a scanning rate of 1 deg. C min^{-1}. Continuous lines are fits to a two-state unfolding transition accompanied by dissociation (see Material and Methods; and equations (A11)-(A13)). The dotted line is the heat capacity of the unfolded state calculated from the amino acid sequence according to Makhatadze & Privalov (1990).[66]

same unfolding enthalpies are obtained also with n fixed at 3 (equations (A2), (A3), and (A13)). The ratio $\Delta H_{vH}/\Delta H_{cal}$ is 1.05 ± 0.5 (mean from 12 measurements). The good correspondence between enthalpies calculated by statistical thermodynamic procedures, by simple van't Hoff considerations, and by direct integration of the excess heat absorption peak, indicates that unfolding is well described by the two-state model.

Table 2. Thermodynamic parameters from thermal unfolding of T582I measured by circular dichroism and differential scanning calorimetry

	CD		DSC						
Concentration[a] (μM)	T_m^b (K)	ΔH_m^c	T_{max}^d (K)	ΔH_{cal}^e	ΔH_{vH}^f	ΔH_{mean}^g	$T_{0.5}^h$ (K)	ΔH_{fit}^i	$\Delta H_{vH}/\Delta H_{cal}$
4.9	340	510							
4.9 (0.44 M urea)	337.8	470.7							
4.9 (0.88 M urea)	335.1	454							
4.9 (0.45 M GdmCl)	333.4	439							
4.9 (0.63 M GdmCl)	328.6	396							
4.9 (0.9 M GdmCl)	325.1	374							
9.7	342.8	510							
33.6	347.8	596							
43.6	348.5	540							
57.1	349	525							
57.1			351.3	642	618	626	350.3	610	0.96
95.7			352.4	524	558	546	351	564	1.06
99.6[j]			351.8	548	578	567	350.8	580	1.05
99.6			352	598	585	589	350.7	585	0.98
109.3			352.4	583	605	597	351.9	618	1.04
109.3[k]			353	507	556	540	351.1	560	1.09

All values are per mol of trimer; experiments were done in PBS; values are ΔH in kJ mol^{-1}; maximal error of $\Delta H \leqslant 10\,\%$; error of transition temperature <1 K.

[a] Total peptide concentration in monomer equivalents.

[b] Temperature of the transition midpoint from CD experiments ($f_M = 0.5$).

[c] Transition enthalpy at T_m.

[d] Temperature of the maximum of the heat capacity trace ($f_M = 0.59$-0.61).

[e] Calorimetric enthalpy calculated by integration of the excess heat capacity peak.

[f] van't Hoff enthalpy calculated according to equation (A10).

[g] Mean weighted enthalpy calculated as $\Delta H_{mean} = 0.65\Delta H_{vH} + 0.35\Delta H_{cal}$.

[h] Temperature of the midpoint of heat release.

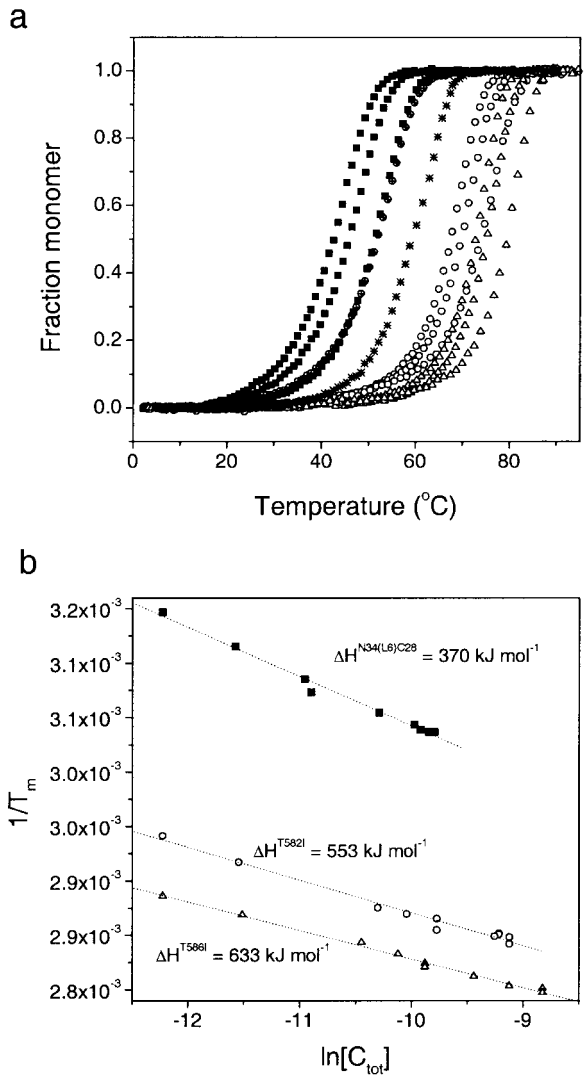

Figure 4. Concentration dependence of thermal unfolding transitions. (a) Normalized melting curves from CD unfolding experiments. Data collected for N34(L6)C28 (squares), T582I (circles), and T586I (triangles) are presented as fraction monomer calculated according to equations (A1)-(A4). Peptide concentrations are 5, 10, and 50 μM (left to right). Unfolding profiles in the presence of 0.9 M GdmCl are shown for T582I (hatched circles) and T586I (asterisks). (b) Variation of the transition temperature with peptide concentration; N34(L6)C28 (squares), T582I (circles), T586I (triangles). Dotted lines are best fits according to:

$$\frac{1}{T_m} = -\frac{2 \times R}{\Delta H_m} + const$$

The numbers are the van't Hoff enthalpies calculated from the slopes.

The partial specific heat capacity of the folded state at 25 °C is the same for the three trimers, 1.7 J K^{-1} g^{-1}, and increases linearly with the temperatures at 7×10^{-3} J K^{-2} g^{-1}. These two values are characteristic for small compact protein domains,[58,59] demonstrating that the trimer-of-hairpins is well packed and does not undergo large fluctuations at temperatures where the folded state dominates. Above the main thermal transition, the heat capacity traces of the unfolded proteins display negligible temperature-dependence.

Isothermal solvent-denaturation experiments

Thermodynamic stability and two-state folding of N34(L6)C28, T582I, and T586I was assessed in yet another way by using GdmCl and urea as denaturants. The equilibrium transitions were followed by monitoring the change of $[\theta]_{222}$ at four different temperatures between 4 and 40 °C. Figure 5 shows normalized unfolding curves obtained at 22 °C with 5 μM peptide. The unfolding reaction is described accurately by the combined equations (A1)-(A3), (A7), and (A8) for trimer-to-monomer unfolding. The transition midpoints of the isoleucine variants are shifted to significantly higher denaturant concentrations. For example, at 22 °C, $[\text{urea}]_{1/2}$ is 1.1 M for N34(L6)C28, 4.0 M for T582I, and 4.8 M for T586I. Table 4 shows the free energies of unfolding, ΔG_{unf}, calculated by the linear extrapolation method, which was adapted to a monomer-trimer equilibrium, and the dependence of ΔG_{unf} on the denaturant concentration, m_D. The ΔG_{unf} values from urea and GdmCl unfolding are very similar, indicating no significant electrostatic contribution to the stability of the trimer-of-hairpins. There is almost no change of ΔG_{unf} between 5 and 40 °C, and m_D values calculated from GdmCl-induced unfolding experiments are identical within error for the three proteins and show no appreciable variation with temperature. N34(L6)C28 seems more sensitive to unfolding in urea than the isoleucine mutants (compare m_D values in Table 4) but the significance of this observation is not clear.

Trimeric N34(L6)C28 contains nine tryptophan residues clustered near the C-terminal part of the N34 coiled-coil and the N-terminal part of the C28 helices. We used the shift of the fluorescence emission maximum to follow denaturant unfolding. The fraction of monomer calculated from the shift of the emission maximum parallels the fraction of monomer calculated from the change of $[\theta]_{222}$, a further strong support for the two-state model of unfolding (Figure 5(a)).

Changes in free energy

The calculated stability curves of N34(L6)C28, T582I, and T586I are compared in Figure 6. The free energy of unfolding, described by equation (A6), is maximal around 20 °C and decreases at lower and higher temperatures. Because of the high conformational stability, cold denaturation is not actually observed. At 3 °C and 5 μM peptide, the lowest experimental temperature and concentration used, only 5 % of N34(L6)C28 is unfolded.

Table 3. Thermodynamic parameters from thermal unfolding of T586I measured by circular dichroism and differential scanning calorimetry

	CD		DSC						
Concentration[a] (μM)	T_m^b (K)	ΔH_m^c	T_{max}^d (K)	ΔH_{cal}^e	ΔH_{vH}^f	ΔH_{mean}^g	$T_{0.5}^h$ (K)	ΔH_{fit}^i	$\Delta H_{vH}/\Delta H_{cal}$
4.9	346.5	577							
4.9 (0.88 M urea)	340.6	612							
4.9 (1.76 M urea)	334.8	484							
4.9 (0.22 M GdmCl)	342.7	606							
4.9 (0.9 M GdmCl)	332.2	476							
4.9 (1.12 M GdmCl)	328.6	440							
4.9 (1.34 M GdmCl)	324.4	409							
10	348.6	601							
29	351.7	611							
40.2	353	590							
51.3	354.1	600							
51.3			355.9	745	725	730	354.5	727	0.97
79.5			357	600	682	653	355.6	685	1.13
109.1			357.9	634	697	675	356.7	700	1.1
147			358.6	740	720	727	357	715	0.97
147[j]			358.7	642	684	669	357.5	685	1.06

All values are per mol of trimer; experiments were done in PBS; ΔH values are in kJ mol^{-1}; maximal error of $\Delta H \leqslant 10\,\%$; error of transition temperature <1 K.

[a] Total peptide concentration in monomer equivalents.

[b] Temperature of the transition midpoint from CD experiments ($f_M = 0.5$).

[c] Transition enthalpy at T_m.

[d] Temperature of the maximum of the heat capacity trace ($f_M = 0.59$-0.61).

[e] Calorimetric enthalpy calculated by integration of the excess heat capacity peak.

[f] van't Hoff enthalpy calculated according to equation (A10).

[g] Mean weighted enthalpy calculated as $\Delta H_{mean} = 0.65\Delta H_{vH} + 0.35\Delta H_{cal}$.

[h] Temperature of the midpoint of heat release.

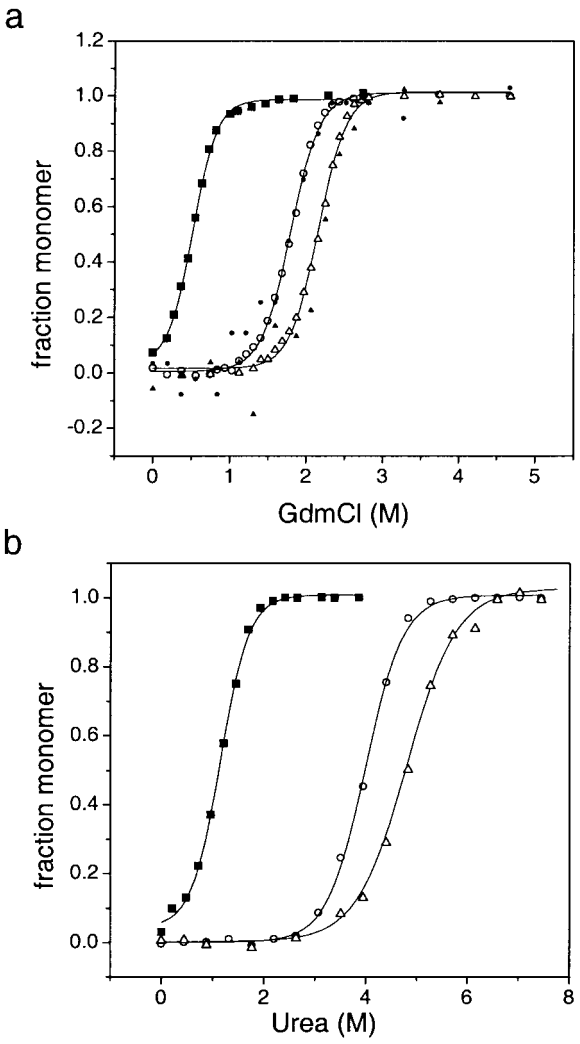

Figure 5. Equilibrium isothermal unfolding of N34(L6)C28 (squares), T582I (circles) and T586I (triangles) by chemical denaturants. Normalized unfolding curves recorded in PBS at 22 °C with 5 μM total monomer concentration in the presence of (a) GdmCl and (b) urea. The symbols are the experimental data and the continuous lines are calculated according to the combined equations (A1)-(A3), (A7) and (A8). Small symbols in (a) are fraction of monomer calculated from spectral shift of the intrinsic tryptophan fluorescence emission maximum.

The calculated stability curves of Figure 6 much depend on the quality of the isothermal low-temperature data.[60,61] To check the accuracy of the fitted $\Delta G_{unf}(T)$ function, we calculate the concentration dependence of T_m for the two-state trimer-monomer equilibrium. K_{unf} relates to ΔG_{unf} by:

$$K_{unf}(T) = \exp[-\Delta G_{unf}(T)/RT]$$

Since at T_m:

$$K_{unf}(T) = 3 \times f_M^3 \times C_{tot}^2/(1 - f_M)$$

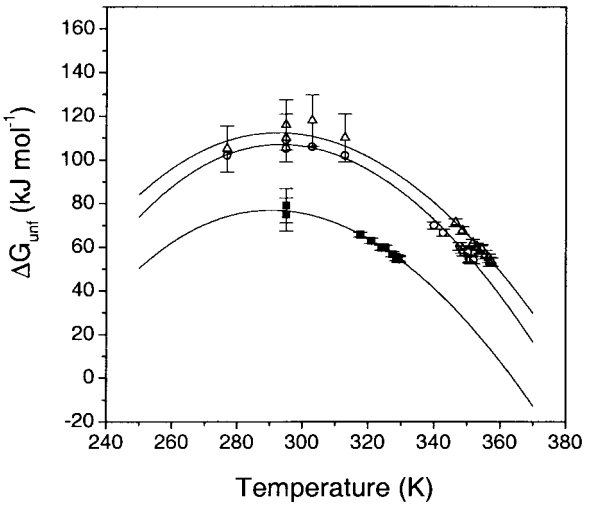

Figure 6. Calculated stability curves for N34(L6)C28 (squares), T582I (circles), and T586I (triangles). Data below 310 K are from isothermal denaturant-induced unfolding experiments. Data at higher temperature are from thermal unfolding experiments. The stability curves were calculated by non-linear least-squares fits using equation (A6).

and $f_M = 0.5$, the total concentration at which the system is half unfolded is $C_{tot} = (K_{unf}/0.75)^{1/2}$. Figure 7 shows very good correspondence between calculated and measured T_m. Thus, the calculated stability curves are reliable estimates of the trimer stability.[42,44]

Replacement of a buried Thr by Ile markedly increases the stability of the trimer-of-hairpins; Thr586 is more sensitive to the mutation than Thr582. The stability profiles have the same shape as that of N34(L6)C28 (Figure 6), since the Thr-to-Ile substitutions do not significantly alter the unfolding heat capacity and the difference in ΔH_{unf} is small (see below). The unfolding free energy of the isoleucine variants is higher in the entire accessible temperature range. To visualize the thermodynamic changes caused by the Thr-to-Ile substitution, we calculate $\Delta\Delta E_{unf} = \Delta E_{unf}^{T/I} - \Delta E_{unf}^{SIVgp41}$, where $\Delta E = \Delta G$, ΔH or $T\Delta S$ (Figure 8(a)). $\Delta\Delta E_{unf}$ values in Figure 8(b) are calculated at the mean experimental temperature, 62 °C, where the error of ΔC_p is minimal. Both Thr-to-Ile substitutions exhibit a similar $\Delta\Delta G_{unf}$.

Enthalpic and entropic contributions to $\Delta\Delta G_{unf}$

Unexpectedly, partitioning of the stabilizing $\Delta\Delta G$ reveals different enthalpic and entropic contributions to high stability (Figure 8). T582I is stabilized by a large decrease of the unfolding entropy ($T\Delta\Delta S_{unf} < 0$), which is partly compensated by a decrease of the unfolding enthalpy $\Delta\Delta H_{unf} < 0$). Entropic stabilization is only half as

Table 4. Thermodynamic parameters from isothermal denaturant-induced unfolding

	Temperature (K)	$[D]_{1/2}$ (M)[a]	$-m_D$ (kJ mol^{-1} M^{-1})[b]	ΔG_{unf} (kJ mol^{-1})[c]
N34(L6)C28				
Urea	295.15	1.1	15.0	79
GdmCl	95.15	0.52	27.6	74.7
T582I				
Urea	295.15	3.98	12.6	105
GdmCl	278.15	1.64	27	102
	295.15	1.79	24.5	109
	303.15	1.62	26.9	106
	313.15	1.42	27.8	103
			Mean 26.6	
T586I				
Urea	295.15	4.8	9.7	110
GdmCl	278.15	2.07	23	105
	295.15	2.15	25.6	116
	303.15	2.08	26.8	119
	313.15	1.92	24	110
			Mean 24.9	

Experiments were done in PBS. Total monomer concentration was 5-5.3 μM. Listed values were calculated according to the combined equations (A1)-(A3) and (A7)-(A9).

[a] Denaturant concentration at which the transition is half complete ($f_M = 0.5$). The error is ~0.1 M.

[b] Error of m_D is 1 (urea data) and 2.5 (GdmCl data) kJ mol^{-1} M^{-1}.

[c] Maximal possible error of ΔG_{unf} due to the uncertainty in $[D]_{1/2}$ and m_D is 10 %.

large for T586I, which is also stabilized by a small favorable enthalpic term ($\Delta\Delta H_{unf} > 0$).

Heat capacity changes

A rigorous thermodynamic description of the unfolding process requires knowledge of the heat capacity change, ΔC_p, accompanying the unfolding transition.[62] We have determined ΔC_p in four different and independent ways.

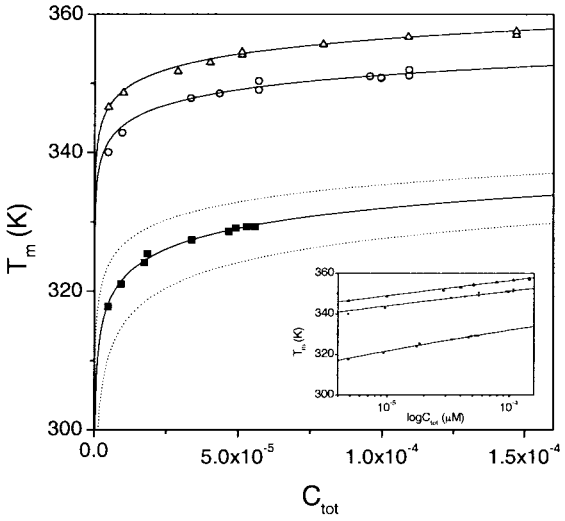

Figure 7. Concentration dependence of the unfolding transition temperature T_m where the protein is half unfolded ($f_M = 0.5$). Experimental T_m values obtained by CD and DSC are shown for N34(L6)C28 (squares), T582I (circles), and T586I (triangles). The continuous lines are the modeled dependencies calculated from the temperature variation of ΔG_{unf} as explained in the text. Dotted lines were calculated assuming a 10 % error of ΔG_{unf}. Inset: the same data plotted on a semi-logarithmic scale.

Kirchhoff plots

The slope of a plot of ΔH_m against T_m is $\partial\Delta H_m/\partial T_m = \Delta C_p$. The corresponding plots are shown in Figure 9 and the following values of ΔC_p are obtained from the slopes shown in the Figure: $\Delta C_p = 8.1(\pm 2)$ kJ K^{-1} mol^{-1} for N34(L6)C28; $\Delta C_p = 7.9(\pm 0.7)$ kJ K^{-1} mol^{-1} for T582I; and $\Delta C_p = 8.4(\pm 0.8)$ kJ K^{-1} mol^{-1} for T586I. These values are identical within error. The large variation of T_m and ΔH_m shown in Figure 9 is achieved by performing thermal unfolding experiments in the presence of low concentrations of GdmCl and urea. This procedure is not devoid of problems, since the enthalpy and heat capacity of denaturant binding to proteins is slightly negative and may lower the apparent ΔC_p of unfolding.[63–65] Fortunately, this effect on the slopes shown in Figure 9 is negligible for the following reasons. (i) At a given temperature, the enthalpies measured in GdmCl and urea are the same (Tables 2 and 3). If the denaturant effect were considerable, the measured enthalpies should be different, since the number of denaturant-binding sites and the molar enthalpy of binding differ for GdmCl and urea. (ii) The following relationship holds at constant peptide concentration:

$$\Delta H_{app}(T^D) = \Delta H(T^D) + \delta\Delta H(T^D) = \Delta H(T_R^W) + \delta\Delta H(T_R^W) + \Delta C_p \times (T^D - T_R^W) \quad (1a)$$

ΔH_{app} (T^D) is the unfolding enthalpy at the melting temperature T^D in the presence of denaturant;

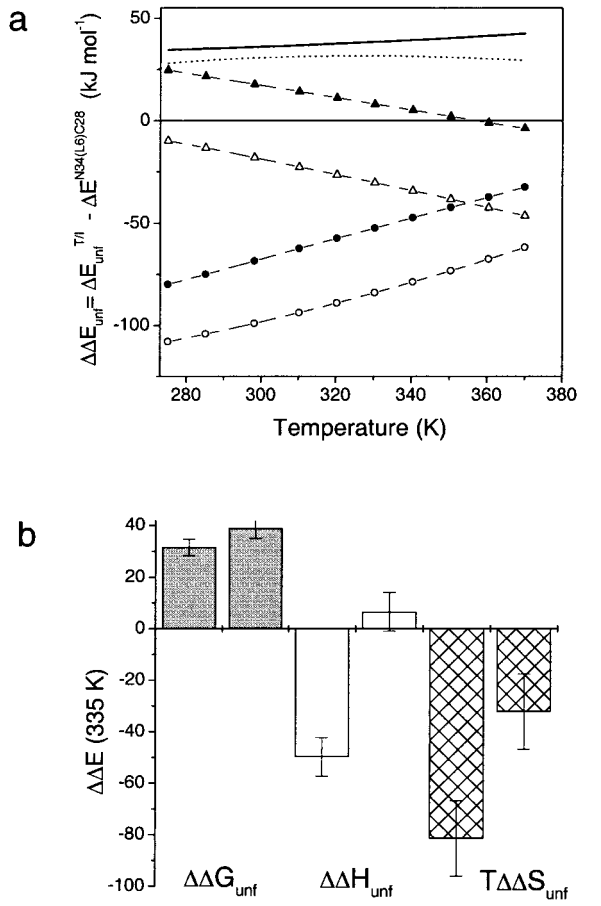

Figure 8. (a) Change of thermodynamic unfolding parameters caused by the Thr-to-Ile substitution in T582I and T586I. $\Delta\Delta E$ was calculated using N34(L6)C28 as a reference. Stabilization is indicated by $\Delta\Delta G_{unf} > 0$, $\Delta\Delta H_{unf} > 0$, and $T\Delta\Delta S_{unf} < 0$. Dotted line, $\Delta\Delta G^{T582I}$; continuous line, $\Delta\Delta G^{T586I}$; filled circles, $\Delta\Delta H^{T582I}$; open circles, $T\Delta\Delta S^{T582I}$; filled triangles, $\Delta\Delta H^{T586I}$; open triangles, $T\Delta\Delta S^{T586I}$. Functions were calculated using ΔC_p derived from the stability curves (Figure 6). (b) $\Delta\Delta E$ at 62 °C, the median experimental temperature.

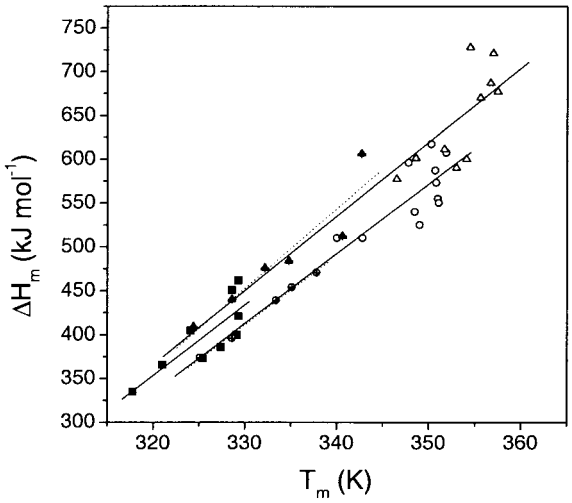

Figure 9. Kirchoff's plot analysis of CD and DSC thermal unfolding experiments performed at pH 7.0 at varying peptide concentrations in the presence and absence of chemical denaturants (data from Tables 1, 2, and 3). N34(L6)C28 (squares), T582I (circles) and T586I (triangles). Data collected in the presence of low concentrations of GdmCl and urea are represented by hatched symbols. Continuous lines are linear best fits from which the heat capacity changes were calculated. Dotted lines are linear fits considering data collected in the presence of denaturant only. Errors of ΔC_p are of the order of 1.5 kJ K^{-1} mol^{-1} (see Error Analysis in Appendix).

$\Delta H(T^D)$ and $\Delta H(T_R^W)$ are the ''true'' unfolding enthalpies at T^D and at an arbitrary reference temperature T_R^W, respectively; $\delta\Delta H(T^D)$ and $\delta\Delta H(T_R^W)$ are the enthalpic contributions of denaturant binding. T^D can be substituted by the linear function $T^D = t \times [D] + T_R^W$, t describing the sensitivity of the melting temperature on the denaturant concentration [D]. If T_R^W is the melting temperature in plain buffer, $\delta\Delta H(T_R^W) = 0$ and equation (1a) simplifies to:

$$\Delta H_{app}(T^D) = \Delta H(T^D) + \delta\Delta H(T^D)$$
$$= \Delta H(T_R^W) + \Delta C_p \times t \times [D] \quad (1b)$$

Analysis of experimental $\Delta H_{app}(T^D)$ as a function of [D] by equation (1b) yields the same ΔC_p values as those obtained from the slopes of Figure 9. Also, $\Delta H(T_R^W)$ equals the unfolding enthalpy measured directly, in the absence of denaturants. (iii) Kirchhoff plots from data collected in plain buffer and in the presence of denaturants have the same slopes. (iv) From the slopes of the regression lines in Figure 4(b), ΔH_{vH} of 370, 553, and 633 kJ mol^{-1} are calculated for N34(L6)C28, T582I, and T586I, respectively. The corresponding values derived from Figure 9 are 380, 545, and 640 kJ mol^{-1}.

ΔC_p from global fits

From the non-linear best fits represented by continuous lines in Figure 6 the following values are obtained: $\Delta C_p = 9(\pm 1.5)$ for N34(L6)C28, $\Delta C_p = 9.8(\pm 0.6)$ for T582I, and $\Delta C_p = 8.7(\pm 0.7)$ kJ K^{-1} mol^{-1} for T586I. These values are also the same within error and are only slightly higher than the ΔC_p values from the Kirchhoff plots of Figure 9. Therefore, we can conclude that ΔC_p values calculated from the temperature dependence of ΔH_{unf} and ΔG_{unf} are all very similar with a mean of 8.7(±0.6) (SD) kJ K^{-1} mol^{-1}.

ΔC_p from DSC traces

Extrapolation of the heat capacity traces of the folded and unfolded states into the transition zone (Figure 3(b)) yields another estimate of ΔC_p. The value obtained, which is ΔC_p at the transition tem-

perature T_m, is close to zero. This unexpected observation suggests that the thermally unfolded state is still compact and not well hydrated as in a fully extended polypeptide. The heat capacity of the latter can be calculated by summing up the side-chain and backbone heat capacities for the amino acid sequence of N34(L6)C28.[58,66] The calculated heat capacity of the extended and fully hydrated peptide chain is indeed much higher than the experimental trace (dotted and continuous lines in Figure 3(b)). At 25 °C, the heat capacity change with respect to the fully unfolded chain is 11 kJ K^{-1} mol^{-1}, larger than ΔC_p obtained by Kirchhoff analysis (Figure 9) and global fitting (Figure 6). As a test for the apparent compact structure of the thermally unfolded state, the DSC experiment with T586I is repeated in the presence of non-denaturing amounts of GdmCl, since this denaturant is known to promote unfolding and hydration of the peptide chain. Indeed, ΔC_p at the transition midpoint of thermal unfolding is 4.7 kJ K^{-1} mol^{-1} in 1 M GdmCl and 6 kJ K^{-1} mol^{-1} in 1.6 M GdmCl.

Semi-empirical calculation of ΔC_p from surface exposed on unfolding

ΔC_p can be estimated from the amount of polar and non-polar surface exposed when the trimer-of-hairpins unfolds into monomers, according to the semi-empirical relationship:

$$\Delta C_p = a_{np}\Delta ASA_{np} + a_{pol}\Delta ASA_{pol} + a_{ar}\Delta ASA_{ar}$$

where ΔASA_{np}, ΔASA_{pol}, and ΔASA_{ar} are the non-polar, polar, and aromatic surface differences between folded trimer and fully unfolded monomers, and a_{np}, a_{pol}, and a_{ar} are constants based on different parametrization schemes.[58,59,67] There is no high-resolution crystal structure of N34(L6)C28 available but the structures of the slightly larger SIV N36(L6)C34 and of the analogous HIV-1 N34(L6)C28 are known and are very similar to each other with an rmsd of C^α-atoms of only 0.97 Å.[23,24] Using the structure of HIV-1 N34(L6)C28 and of SIV N36(L6)C34 trimmed to the size of the N34(L6)C28, one calculates about 12,000 $Å^2$ of non-polar surface, from which 6% come from aromatic groups, and about 6000 $Å^2$ of polar surface to be exposed upon complete unfolding of the trimer-of-hairpins. From this, the estimated ΔC_p is 12-16 kJ K^{-1} mol^{-1}, the calculated value depending on the parameters a_{np}, a_{pol}, and a_{ar} used in the calculation.[58,59,67] This estimate is not far from $\Delta C_p = 11$ kJ K^{-1} mol^{-1} estimated from the difference between the calculated and measured DSC traces at 25 °C (continuous and dotted lines in Figure 3(b)), which corresponds to ΔC_p for the complete unfolding of the trimer into fully hydrated peptide chains.

In concluding this section, we note that the four methods to obtain ΔC_p yield a value of 8.7(±0.6) kJ K^{-1} mol^{-1} for the thermally unfolded state and of 12-16 kJ K^{-1} mol^{-1} for complete unfolding; the latter range is only a crude estimate based on analogous crystal structures and on heat capacities calculated from amino acid transfer data.

Discussion

Thermodynamics of trimer-of-hairpins unfolding

This study provides the first detailed thermodynamic analysis of a complex trimer-of-hairpins protein. An important finding is a low heat capacity change for thermal unfolding of the trimer-of-hairpins structure into three unfolded peptide chains. Interestingly, lower than expected heat capacity changes have been reported for other oligomeric proteins.[34,38,39,68–70] Since ΔC_p is dominated by hydration effects, low experimental ΔC_p has been attributed to incomplete unfolding resulting in a compact and not fully solvated-denatured state.[59] As seen in Figure 3(b), the heat capacity of the thermally unfolded state is much lower than ΔC_p calculated from the amino acid sequence assuming a completely solvated polypeptide chain. This conclusion is supported by the results of DSC experiments performed in the presence of low GdmCl concentration, which reveal a higher apparent ΔC_p. Furthermore, m_D-values for chemical denaturation are of the expected magnitude, or even larger, than calculated for complete unfolding (data not shown).[71] Thus, the heat-denatured state is very likely to retain residual structure that is destroyed only by chemical denaturants. However, one should also consider that the folded trimer-of-hairpins could have a slightly greater heat capacity than a compact, monomeric protein.[72] Vibrational modes and molecular fluctuations can be significant between the subunits of non-covalently associating systems and can increase the heat capacity of the folded state leading to a smaller ΔC_p.[73–75] Whatever the true cause(s) of the moderate heat capacity change, N34(L6)C28 and its isoleucine variants unfold according to a ''fixed two-state'' model in which the high-temperature unfolded ensemble is energetically indistinguishable from and has the same thermodynamic character as the denatured ensemble in the limit of zero denaturant concentration.[76]

To compare thermodynamic data pertaining to multimeric and monomeric proteins, respectively, the specific thermodynamic quantities expressed per mol of residue (or per gram of protein) are helpful. The intrinsic stability of N34(L6)C28 at 25 °C is 370 J (mol residue)$^{-1}$. This value is within the range of 200-600 J (mol residue)$^{-1}$ observed for other proteins.[59] The stability markedly increases to ~550 J (mol residue)$^{-1}$ upon the replacement of Thr by Ile. For many proteins of different size and molecular architecture, the specific enthalpies and entropies of unfolding appear to be similar.[59] For the three proteins studied here, the specific enthal-

py at 62 °C amounts to ~2.3 kJ (mol residue)$^{-1}$, which is lower than the mean value of 3.5(±1) kJ (mol residue)$^{-1}$ calculated for several globular proteins at this temperature. The specific unfolding entropy is ~6 J K^{-1} (mol residue)$^{-1}$, which also is lower than the 9(±1.5) J K^{-1} (mol residue)$^{-1}$ typically observed at this temperature. Although such comparison may be of limited significance, it is in line with a compact thermally unfolded state, which retains residual interactions and whose entropy is lower than that of the fully hydrated polypeptide chain.

Large stabilization of coiled coil by a single Thr-to-Ile replacement

Substitution of the buried triad of threonine residues by isoleucine residues stabilizes the trimer-of-hairpins by 30-35 kJ mol^{-1}, a mean stabilization per residue of 10-12 kJ mol^{-1}. This is a high gain of stability among mutations involving hydroxyl group-containing side-chains like Ser-to-Ala or Thr-to-Val.[77–82] Stabilization is not caused by a gain in helix stability, which for Thr-to-Ile mutation is only of the order of 1.1 kJ mol^{-1}.[83] Since both Thr582 and Thr586 are completely buried at the inter-helical interface, the Ile variants expose more apolar surface (~200 Å^2) and less polar surface (~100 Å^2). The stabilization due to the hydrophobic effect (including mutation-related changes in both molecular surface hydration and packing interactions) should amount to ~ 6 kJ mol^{-1} (calculated from Table XIII of Makhatadze & Privalov[59]). Without high-resolution structural data for N34(L6)C28 and its mutants, the observed large stabilization is difficult to rationalize. One possibility is that in the parent protein N34(L6)C28, the threonine hydroxyl groups have imperfect polar-polar contacts (e.g. no proper H-bonding) within the mostly apolar environment of the hydrophobic core. This could decrease ΔG_{unf} of the parent protein. In any case, the fact that the increase of ΔG_{unf} is dominated by changes in entropy (Figure 8(b)) would appear to point to the importance of favorable hydration effects in the isoleucine mutants. Notably, however, the equivalent amino acid substitutions studied here are energetically balanced in a different way. Therefore, the isoleucine substitution at the ***a*** or ***d*** position of the N-terminal coiled-coil might have introduced a local perturbation of the structure, thereby changing both the enthalpic packing interactions and entropic content of the folded state. Incidentally, the T582I mutant of the related SIV N36(L6)C34 gp41 core is stabilized by only 6 kJ mol^{-1},perhaps indicating some packing differences in the N-terminal coiled-coil of the two otherwise highly similar trimer-of-hairpins.[55] The energetic non-equivalence of the ***a*** and ***d*** positions in coiled-coils has been demonstrated.[37,47]

Implications for membrane fusion

An influx of structural and functional information on the HIV-1 membrane fusion process indicates that the refolding of the gp41 envelope protein into its fusion-active conformation controls the key process of viral entry.[4,84] According to present theories, this conformational activation involves the transition from a labile, as yet undefined, native state to the fusogenic trimer-of-hairpins structure, which then mediates viral-cell membrane fusion. It would appear that as the helical-hairpin complex is assembled and simultaneously the fusion peptide is inserted into the target membrane, a ready source of energy could be made available for overcoming the activation energy needed to bring two lipid bilayers into intimate approximation at the fusion site. Our calorimetric and CD studies show that the recombinant N34(L6)C28 model of the SIV gp41 core undergoes a cooperative two-state unfolding transition by heat or upon addition of chemical denaturants. Thermodynamic functions describing this process allow us to calculate the energetics of trimer-of-hairpins formation from the experimental data over a broad temperature range and characterize the factors responsible for the folding of the gp41 core to its fusogenic conformation. Our results show that the trimeric N34(L6)C28 complex has a maximum of thermodynamic stability of 76 kJ/mol at around 25 °C. Since the trimeric structural domain of the full-length ectodomain of gp41 has been truncated by nearly a quarter in N34(L6)C28, this estimate is perhaps a lower bound. The fusion-active structure of the gp41 membrane protein is expected to be further stabilized by its covalent attachment to both the viral and cellular membranes, so that the thermal stability characterized in the present study is likely to mark the lower limit of stability of the activated gp41 molecule.

The N-terminal coiled-coil sequence of gp41 is one of the most highly conserved regions within the primate immunodeficiency virus envelope proteins, which otherwise exhibit considerable genetic diversity, even among closely related isolates.[15–17] There is only one non-conservative substitution in the ***a*** position of the N-terminal heptad repeat (Thr586 in SIV, and Ile in the corresponding position of HIV-1). The folding and stability of the HIV-1 gp41 ectodomain core bearing mutations in this position correlate with severity of the *in vivo* phenotypes observed in cells expressing the mutant envelope glycoproteins.[85,86] Altogether, the evidence suggests that formation of the N-terminal three-stranded coiled-coil occurs as an early event in the gp41 refolding process required for initiating membrane fusion. Our results show that the replacement of each of the two polar residues, Thr582 and Thr586, at the trimeric coiled-coil interface by the apolar residue isoleucine stabilizes the trimer-of-hairpins by 30-35 kJ mol^{-1}. These results suggest that the buried polar interactions within the N-terminal coiled-coil may serve to tip the balance

between the metastable prefusogenic and most stable fusogenic states of gp41 by destabilizing the fusogenic structure, as opposed to stabilizing the labile prefusogenic conformation. The release of energy for lipid bilayer fusion from the helical-hairpin assembly is therefore likely to be a tightly regulated process, thereby allowing structural rearrangements in gp41 to occur in a concerted fashion. Further thermodynamic, structural, and functional studies of the gp41 mutants are required for addressing this and other essential mechanistic questions about the retrovirus-mediated membrane fusion reaction.

Material and Methods

Gene construction and protein production

Plasmid pN34/C28, encoding the N34(L6)C28 model for the SIV gp41 ectodomain core, was derived from pN36/C34.[55] Mutations were introduced into pN34/C28 by single-stranded mutagenesis[87] and verified by DNA sequencing. Standard recombinant DNA techniques were used.[88] All recombinant proteins were expressed in *Escherichia coli* BL21(DE3)/pLysS using the phage T7 expression system.[89] Cells, freshly transformed with an appropriate plasmid, were grown to late log phase. Protein expression was induced by addition of 0.5 mM isopropylthio-β-D-galactoside (IPTG). After growth for another three hours at 37 °C, the bacteria were harvested by centrifugation, and the cells were lysed by glacial acetic acid as described.[20] Proteins were purified from the soluble fraction to homogeneity by reverse-phase HPLC, using a Vydac C-18 preparative column and a linear gradient of acetonitrile containing 0.1 % (v/v) trifluoroacetic acid. The identities of peptides were confirmed by mass spectrometry (Perceptive Biosystems Voyager Elite), and all molecular masses were found to be within 2 Da of the expected molecular mass. Peptide concentrations were determined by measurement of absorbance at 280 nm in 6 M GdmCl.[90]

Buffers

All experiments were conducted in standard PBS buffer (8.3 mM Na_2HPO_4, 1.47 mM KH_2PO_4 (pH 7.0), 137 mM NaCl, 2.7 mM KCl; $I = 164$ mM). The pH of buffers containing urea or GdmCl was adjusted after adding the denaturant. All chemicals were of analytical grade and were used without further purification.

Sedimentation equilibrium

Sedimentation equilibrium analysis was performed on a Beckman XL-A analytical ultracentrifuge as described.[91] Protein solutions were dialyzed overnight against 50 mM sodium phosphate (pH 7.0), 150 mM NaCl, loaded at initial concentrations of 10, 30, and 100 μM, and analyzed at rotor speeds of 20,000 and 23,000 rpm at 20 °C (An-Ti rotor and six-sectored equilibrium centrifugation/centerpieces). Data sets were fitted to a single-species model.[92] Protein partial specific volume and solvent density were calculated with constants from Laue *et al.*[93] Molecular masses were all within 10 % of those calculated for an ideal trimer, with no systematic deviation of the residuals.

CD spectroscopy

CD measurements were performed on a Jasco-715 spectropolarimeter equipped with a computer-controlled waterbath, using thermostated cuvettes of 0.02, 0.1 or 1 cm pathlength. Thermal unfolding curves were measured by continuously measuring the ellipticity at 222 nm between 3 and 95 °C at a scan rate of 0.9 deg. C min^{-1} and with data collection every 20 seconds. Reversibility of unfolding was checked by two cycles of heating and cooling or by following the time-evolution of the CD signal for more than one hour at a temperature close to the midpoint of the spectral change and was always better than 95 %. Conformational changes induced by urea and GdmCl were monitored at 222 nm. Data were sampled for three minutes at the experimental temperature after incubation of ~5 μM peptide for 12-15 hours at the desired denaturant concentration. No further signal change was observed after 48 hours of incubation. Analysis of heat and denaturant-induced unfolding curves followed the formalism describing a simple two-state conformational transition between folded trimer, T, and unfolded random-coil monomer, M. The derivation of all equations used is detailed in the Appendix.

DSC measurements

DSC experiments were performed on the VP-DSC microcalorimeter (MicroCal Inc.) equipped with twin coin-shaped cells of 0.52 ml volume. Technical details and the performance of the instrument have been described.[94] Peptides were dialyzed for 18-24 hours against the same batch of buffer used to establish the baseline. The scan rate in most experiments was 1 deg. C min^{-1}. Scans at heating rates of 0.5 and 1.5 deg. C min^{-1} were performed also and the calculated thermodynamic parameters were independent of the scanning rate within error. Reversibility was routinely checked by two to four cycles of heating and cooling, and was better than 95 % for total peptide concentration up to about 60 μM (0.5 mg/ml) for N34(L6)C28 and 180 μM (1.5 mg/ml) for the T582I and T586I mutants. To test the ''true'' thermodynamic reversibility, peptide samples were heated at 1 deg. C min^{-1} to the temperature corresponding to the maximum of the heat capacity function and were incubated at this temperature. The recorded differential power signal did not show any measurable drift from the equilibrium value for more than one hour of incubation. Subsequent cooling and heating revealed complete reversibility. The calorimetric (model-independent) and effective (model-dependent) unfolding enthalpies were obtained from DSC traces according the equations specified in the Appendix.

Fluorescence spectroscopy

Measurements were made on a Perkin Elmer LS 50B luminescence spectrometer. Spectra were measured in 1 nm steps with one second integration time. Trp emission was monitored between 340 nm and 380 nm upon excitation at 295 nm.

Acknowledgments

We thank Professor H. R. Bosshard for critical comments on the manuscript. This work was supported, in

part, by the Swiss National Science Foundation (grant 3100-055308.98/1) to I.J. and National Institutes of Health grant AI42382 to M.L.

References

1. Hunter, E. & Swanstrom, R. (1990). Retrovirus envelope glycoproteins. *Curr. Topics Microbiol. Immunol.* **157**, 187-253.
2. Luciw, P. A. (1996). Human immunodeficiency viruses and their replication. In *Fields Virology* (Fields, B. N., Knipe, D. M., Howley, P. M., Chanock, R. M., Melinick, J. L., Monath, T. P., Roizman, B. & Strauss, S. E., eds), p. 1881, Lippincott-Raven Publishers, Philadelphia.
3. Berger, E. A., Murphy, P. M. & Farber, J. M. (1999). Chemokine receptors as HIV-1 coreceptors: roles in viral entry, tropism, and disease. *Annu. Rev. Immunol.* **17**, 657-700.
4. Chan, D. C. & Kim, P. S. (1998). HIV entry and its inhibition. *Cell,* **93**, 681-684.
5. Bullough, P. A., Hughson, F. M., Skehel, J. J. & Wiley, D. C. (1994). Structure of influenza haemagglutinin at the pH of membrane fusion. *Nature,* **371**, 37-43.
6. Carr, C. M., Chaudhry, C. & Kim, P. S. (1997). Influenza hemagglutinin is spring-loaded by a metastable native conformation. *Proc. Natl Acad. Sci. USA,* **94**, 14306-14313.
7. Carr, C. M. & Kim, P. S. (1993). A spring-loaded mechanism for the conformational change of influenza hemagglutinin. *Cell,* **73**, 823-832.
8. Chen, J., Wharton, S. A., Weissenhorn, W., Calder, L. J., Hughson, F. M., Skehel, J. J. & Wiley, D. C. (1995). A soluble domain of the membrane-anchoring chain of influenza virus hemagglutinin (HA2) folds in *Escherichia coli* into the low-pH-induced conformation. *Proc. Natl Acad. Sci. USA,* **92**, 12205-12209.
9. Eckert, D. M., Malashkevich, V. N., Hong, L. H., Carr, P. A. & Kim, P. S. (1999). Inhibiting HIV-1 entry: discovery of D-peptide inhibitors that target the gp41 coiled-coil pocket. *Cell,* **99**, 103-115.
10. Ferrer, M., Kapoor, T. M., Strassmaier, T., Weissenhorn, W., Skehel, J. J., Oprian, D., Schreiber, S. L., Wiley, D. C. & Harrison, S. C. (1999). Selection of gp41-mediated HIV-1 cell entry inhibitors from biased combinatorial libraries of non-natural binding elements. *Nature Struct. Biol.* **6**, 953-960.
11. Kilby, J. M., Hopkins, S., Venetta, T. M., DiMassimo, B., Cloud, G. A., Lee, J. Y., Alldredge, L., Hunter, E., Lambert, D., Bolognesi, D., Matthews, T., Johnson, M. R., Nowak, M. A., Shaw, G. M. & Saag, M. S. (1998). Potent suppression of HIV-1 replication in humans by T-20, a peptide inhibitor of gp41-mediated virus entry. *Nature Med.* **4**, 1302-1307.
12. Sodroski, J. G. (1999). HIV-1 entry inhibitors in the side pocket. *Cell,* **99**, 243-246.
13. Stegmann, T., Delfino, J. M., Richards, F. M. & Helenius, A. (1991). The HA2 subunit of influenza hemagglutinin inserts into the target membrane prior to fusion. *J. Biol. Chem.* **266**, 18404-18410.
14. Tsurudome, M., Gluck, R., Graf, R., Falchetto, R., Schaller, U. & Brunner, J. (1992). Lipid interactions of the hemagglutinin HA2 NH2-terminal segment during influenza virus-induced membrane fusion. *J. Biol. Chem.* **267**, 20225-20232.
15. Chambers, P., Pringle, C. R. & Easton, A. J. (1990). Heptad repeat sequences are located adjacent to hydrophobic regions in several types of virus fusion glycoproteins. *J. Gen. Virol.* **71**, 3075-3080.
16. Delwart, E. L., Mosialos, G. & Gilmore, T. (1990). Retroviral envelope glycoproteins contain a ''leucine zipper''-like repeat. *AIDS Res. Hum. Retroviruses,* **6**, 703-706.
17. Gallaher, W. R., Ball, J. M., Garry, R. F., Griffin, M. C. & Montelaro, R. C. (1989). A general model for the transmembrane proteins of HIV and other retroviruses. *AIDS Res. Hum. Retroviruses,* **5**, 431-440.
18. Blacklow, S. C., Lu, M. & Kim, P. S. (1995). A trimeric subdomain of the simian immunodeficiency virus envelope glycoprotein. *Biochemistry,* **34**, 14955-14962.
19. Lu, M., Blacklow, S. C. & Kim, P. S. (1995). A trimeric structural domain of the HIV-1 transmembrane glycoprotein. *Nature Struct. Biol.* **2**, 1075-1082.
20. Lu, M. & Kim, P. S. (1997). A trimeric structural subdomain of the HIV-1 transmembrane glycoprotein. *J. Biomol. Struct. Dynam.* **15**, 465-471.
21. Caffrey, M., Cai, M., Kaufman, J., Stahl, S. J., Wingfield, P. T., Covell, D. G., Gronenborn, A. M. & Clore, G. M. (1998). Three-dimensional solution structure of the 44 kDa ectodomain of SIV gp41. *EMBO J.* **17**, 4572-4584.
22. Chan, D. C., Fass, D., Berger, J. M. & Kim, P. S. (1997). Core structure of gp41 from the HIV envelope glycoprotein. *Cell,* **89**, 263-273.
23. Malashkevich, V. N., Chan, D. C., Chutkowski, C. T. & Kim, P. S. (1998). Crystal structure of the simian immunodeficiency virus (SIV) gp41 core: conserved helical interactions underlie the broad inhibitory activity of gp41 peptides. *Proc. Natl Acad. Sci. USA,* **95**, 9134-9139.
24. Tan, K., Liu, J., Wang, J., Shen, S. & Lu, M. (1997). Atomic structure of a thermostable subdomain of HIV-1 gp41. *Proc. Natl Acad. Sci. USA,* **94**, 12303-12308.
25. Weissenhorn, W., Dessen, A., Harrison, S. C., Skehel, J. J. & Wiley, D. C. (1997). Atomic structure of the ectodomain from HIV-1 gp41. *Nature,* **387**, 426-430.
26. Yang, Z. N., Mueser, T. C., Kaufman, J., Stahl, S. J., Wingfield, P. T. & Hyde, C. C. (1999). The crystal structure of the SIV gp41 ectodomain at 1.47 Å resolution. *J. Struct. Biol.* **126**, 131-144.
27. Jiang, S., Lin, K. & Lu, M. (1998). A conformation-specific monoclonal antibody reacting with fusion-active gp41 from the human immunodeficiency virus type 1 envelope glycoprotein. *J. Virol.* **72**, 10213-10217.
28. Kwong, P. D., Wyatt, R., Robinson, J., Sweet, R. W., Sodroski, J. & Hendrickson, W. A. (1998). Structure of an HIV gp120 envelope glycoprotein in complex with the CD4 receptor and a neutralizing human antibody. *Nature,* **393**, 648-659.
29. Rizzuto, C. D., Wyatt, R., Hernandez-Ramos, N., Sun, Y., Kwong, P. D., Hendrickson, W. A. & Sodroski, J. (1998). A conserved HIV gp120 glycoprotein structure involved in chemokine receptor binding. *Science,* **280**, 1949-1953.
30. Furuta, R. A., Wild, C. T., Weng, Y. & Weiss, C. D. (1998). Capture of an early fusion-active conformation of HIV-1 gp41. *Nature Struct. Biol.* **5**, 276-279.
31. Jones, P. L., Korte, T. & Blumenthal, R. (1998). Conformational changes in cell surface HIV-1 envelope glycoproteins are triggered by cooperation between

cell surface CD4 and co-receptors. *J. Biol. Chem.* **273**, 404-409.
32. Munoz-Barroso, I., Durell, S., Sakaguchi, K., Appella, E. & Blumenthal, R. (1998). Dilation of the human immunodeficiency virus-1 envelope glycoprotein fusion pore revealed by the inhibitory action of a synthetic peptide from gp41. *J. Cell Biol.* **140**, 315-323.
33. Hughson, F. M. (1997). Enveloped viruses: a common mode of membrane fusion? *Curr. Biol.* **7**, R565-R569.
34. Backmann, J., Schafer, G., Wyns, L. & Bonisch, H. (1998). Thermodynamics and kinetics of unfolding of the thermostable trimeric adenylate kinase from the archaeon *Sulfolobus acidocaldarius*. *J. Mol. Biol.* **284**, 817-833.
35. Boudker, O., Todd, M. J. & Freire, E. (1997). The structural stability of the co-chaperonin groES. *J. Mol. Biol.* **272**, 770-779.
36. Bowie, J. U. & Sauer, R. T. (1989). Equilibrium dissociation and unfolding of the Arc repressor dimer. *Biochemistry,* **28**, 7139-7143.
37. Jelesarov, I. & Bosshard, H. R. (1996). Thermodynamic characterization of the coupled folding and association of heterodimeric coiled-coils (leucine zippers). *J. Mol. Biol.* **263**, 344-358.
38. Johnson, C. R., Morin, P. E., Arrowsmith, C. H. & Freire, E. (1995). Thermodynamic analysis of the structural stability of the tetrameric oligomerization domain of p53 tumor suppressor. *Biochemistry,* **34**, 5309-53016.
39. Karantza, V., Baxevanis, A. D., Freire, E. & Moudrianakis, E. N. (1995). Thermodynamic studies of the core histones: ionic strength and pH dependence of H2A-H2B dimer stability. *Biochemistry,* **34**, 5988-5996.
40. Kretschmar, M. & Jaenicke, R. (1999). Stability of a homo-dimeric Ca^{2+}-binding member of the beta gamma-crystallin superfamily: DSC measurements on spherulin 3a from *Physarum polycephalum*. *J. Mol. Biol.* **291**, 1147-1153.
41. Li, W. T., Grayling, R. A., Sandman, K., Edmondson, S., Shriver, J. W. & Reeve, J. N. (1998). Thermodynamic stability of archaeal histones. *Biochemistry,* **37**, 10563-10572.
42. Panse, V. G., Swaminathan, C. P., Aloor, J. J., Surolia, A. & Varadarajan, R. (2000). Unfolding thermodynamics of the tetrameric chaperone, SecB. *Biochemistry,* **39**, 2362-2369.
43. Steif, C., Weber, P., Hinz, H. J., Flossdorf, J., Cesareni, G. & Kokkinidis, M. (1993). Subunit interactions provide a significant contribution to the stability of the dimeric four-alpha-helical-bundle protein ROP. *Biochemistry,* **32**, 3867-3876.
44. Thompson, K. S., Vinson, C. R. & Freire, E. (1993). Thermodynamic characterization of the structural stability of the coiled-coil region of the bZIP transcription factor GCN4. *Biochemistry,* **32**, 5491-5496.
45. Todd, M. J., Semo, N. & Freire, E. (1998). The structural stability of the HIV-1 protease. *J. Mol. Biol.* **283**, 475-388.
46. Zhou, N. E., Kay, C. M. & Hodges, R. S. (1992a). Synthetic model proteins. Positional effects of interchain hydrophobic interactions on stability of two-stranded α-helical coiled-coils. *J. Biol. Chem.* **267**, 2664-2670.
47. Zhou, N. E., Kay, C. M. & Hodges, R. S. (1992b). Synthetic model proteins: the relative contribution of leucine residues at the nonequivalent positions of the 3-4 hydrophobic repeat to the stability of the two-stranded α-helical coiled-coil. *Biochemistry,* **31**, 5739-5746.
48. Mateu, M. G. & Fersht, A. R. (1998). Nine hydrophobic side-chains are key determinants of the thermodynamic stability and oligomerization status of tumour suppressor p53 tetramerization domain. *EMBO J.* **17**, 2748-2758.
49. Milla, M. E., Brown, B. M. & Sauer, R. T. (1994). Protein stability effects of a complete set of alanine substitions in Arc repressor. *Nature Struct. Biol.* **1**, 518-523.
50. Steif, C., Hinz, H. J. & Cesareni, G. (1995). Effects of cavity-creating mutations on conformational stability and structure of the dimeric 4-alpha-helical protein ROP: thermal unfolding studies. *Proteins: Struct. Funct. Genet.* **23**, 83-96.
51. Murphy, K. P., Xie, D., Thompson, K. S., Amzel, L. M. & Freire, E. (1994). Entropy in biological binding processes: estimation of translational entropy loss. *Proteins: Struct. Funct. Genet.* **18**, 63-67.
52. Spolar, R. S. & Record, M. T., Jr (1994). Coupling of local folding to site-specific binding of proteins to DNA. *Science,* **263**, 777-784.
53. Yu, Y. H. B., Lavigne, P., Kay, C. M., Hodges, R. S. & Privalov, P. L. (1999). Contribution of translational and rotational entropy to the unfolding of a dimeric coiled-coil. *J. Phys. Chem. ser. B,* **103**, 2270-2278.
54. Caffrey, M., Kaufman, J., Stahl, S., Wingfield, P., Gronenborn, A. M. & Clore, G. M. (1999). Monomer-trimer equilibrium of the ectodomain of SIV gp41: insight into the mechanism of peptide inhibition of HIV infection. *Protein Sci.* **8**, 1904-1907.
55. Ji, H., Bracken, C. & Lu, M. (2000). Buried polar interactions and conformational stability in the simian immunodeficiency virus (SIV) gp41 core. *Biochemistry,* **39**, 676-685.
56. Freire, E. (1989). Statistical thermodynamic analysis of the heat capacity function associated with protein folding-unfolding transitions. *Comm. Mol. Cell. Biophys.* **6**, 123-140.
57. Privalov, P. L. & Potekhin, S. A. (1986). Scanning microcalorimetry in studying temperature-induced changes in proteins. *Methods Enzymol.* **131**, 4-51.
58. Gomez, J., Hilser, V. J., Xie, D. & Freire, E. (1995). The heat capacity of proteins. *Proteins: Struct. Funct. Genet.* **22**, 404-412.
59. Makhatadze, G. I. & Privalov, P. L. (1995). Energetics of protein structure. *Advan. Protein Chem.* **47**, 307-425.
60. Johnson, C. M. & Fersht, A. R. (1995). Protein stability as a function of denaturant concentration: ther thermal stability of barnase in the presence of urea. *Biochemistry,* **34**, 6795-6804.
61. Santoro, M. M. & Bolen, D. W. (1992). A test of the linear extrapolation of unfolding free energy changes over an extended denaturant concentration range. *Biochemistry,* **31**, 4901-4907.
62. Becktel, W. J. & Schellman, J. A. (1987). Protein stability curves. *Biopolymers,* **26**, 1859-1877.
63. Makhatadze, G. I. & Privalov, P. L. (1992). Protein interactions with urea and guanidinium chloride. A calorimetric study. *J. Mol. Biol.* **226**, 491-505.
64. McCrary, B. S., Edmondson, S. P. & Shriver, J. W. (1996). Hyperthermophile protein folding thermodynamics: differential scanning calorimetry and chemical denaturation of Sac7d. *J. Mol. Biol.* **264**, 784-805.

65. Pfeil, W., Gesierich, U., Kleemann, G. R. & Sterner, R. (1997). Ferredoxin from the hyperthermophile *Thermotoga maritima* is stable beyond the boiling point of water. *J. Mol. Biol.* **272**, 591-596.
66. Makhatadze, G. I. & Privalov, P. L. (1990). Heat capacity of proteins. I. Partial molar heat capacity of individual amino acid residues in aqueous solution: hydration effect. *J. Mol. Biol.* **213**, 375-384.
67. Spolar, R. S., Livingstone, J. R. & Record, M. T., Jr (1992). Use of liquid hydrocarbon and amide transfer data to estimate contributions to thermodynamic functions of protein folding from the removal of nonpolar and polar surface from water. *Biochemistry,* **31**, 3947-3955.
68. Arnone, M. I., Birolo, L., Pascarella, S., Cubellis, M. V., Bossa, F., Sannia, G. & Marino, G. (1997). Stability of aspartate aminotransferase from *Sulfolobus solfataricus*. *Protein Eng.* **10**, 237-248.
69. Hagihara, Y., Oobatake, M. & Goto, Y. (1994). Thermal unfolding of tetrameric melittin: comparison with the molten globule state of cytochrome *c*. *Protein Sci.* **3**, 1418-1429.
70. Kaplan, W., Husler, P., Klump, H., Erhardt, J., Sluis-Cremer, N. & Dirr, H. (1997). Conformational stability of pGEX-expressed Schistosoma japonicum glutathione *S*-transferase: a detoxification enzyme and fusion-protein affinity tag. *Protein Sci.* **6**, 399-406.
71. Myers, J. K., Pace, C. N. & Scholtz, J. M. (1995). Denaturant *m* values and heat capacity changes: relation to changes in accessible surface areas of protein unfolding. *Protein Sci.* **4**, 2138-2148.
72. Karantza, V., Freire, E. & Moudrianakis, E. N. (1996). Thermodynamic studies of the core histones: pH and ionic strength effects on the stability of the (H3-H4)/(H3-H4)2 system. *Biochemistry,* **35**, 2037-2046.
73. Jelesarov, I., Crane-Robinson, C. & Privalov, P. L. (1999). The energetics of HMG box interactions with DNA: thermodynamic description of the target DNA duplexes. *J. Mol. Biol.* **294**, 981-995.
74. Privalov, P. L., Jelesarov, I., Read, C. M., Dragan, A. I. & Crane-Robinson, C. (1999). The energetics of HMG box interactions with DNA: thermodynamics of the DNA binding of the HMG box from mouse sox-5. *J. Mol. Biol.* **294**, 997-1013.
75. Tidor, B. & Karplus, M. (1994). The contribution of vibrational entropy to molecular association. The dimerization of insulin. *J. Mol. Biol.* **238**, 405-414.
76. Baskakov, I. V. & Bolen, D. W. (1998). Monitoring the sizes of denatured ensembles of staphylococcal nuclease proteins: implications regarding *m* values, intermediates, and thermodynamics. *Biochemistry,* **37**, 18010-18017.
77. Blaber, M., Lindstrom, J. D., Gassner, N., Xu, J., Heinz, D. W. & Matthews, B. W. (1993). Energetic cost and structural consequences of burying a hydroxyl group within the core of a protein determined from Ala → Ser and Val → Thr substitutions in T4 lysozyme. *Biochemistry,* **32**, 11363-11373.
78. Byrne, M. P., Manuel, R. L., Lowe, L. G. & Stites, W. E. (1995). Energetic contribution of side-chain hydrogen bonding to the stability of staphylococcal nuclease. *Biochemistry,* **34**, 13949-13960.
79. Serrano, L., Kellis, J. T., Jr, Cann, P., Matouschek, A. & Fersht, A. R. (1992). The folding of an enzyme. II. Substructure of barnase and the contribution of different interactions to protein stability. *J. Mol. Biol.* **224**, 783-804.
80. Shirley, B. A., Stanssens, P., Hahn, U. & Pace, C. N. (1992). Contribution of hydrogen bonding to the conformational stability of ribonuclease T1. *Biochemistry,* **31**, 725-732.
81. Takano, K., Yamagata, Y., Funahashi, J., Hioki, Y., Kuramitsu, S. & Yutani, K. (1999). Contribution of intra- and intermolecular hydrogen bonds to the conformational stability of human lysozyme. *Biochemistry,* **38**, 12698-12708.
82. Yutani, K., Ogasahara, K., Tsujita, T. & Sugino, Y. (1987). Dependence of conformational stability on hydrophobicity of the amino acid residue in a series of variant proteins substituted at a unique position of tryptophan synthase alpha subunit. *Proc. Natl Acad. Sci. USA,* **84**, 4441-4444.
83. Pace, C. N. & Scholtz, J. M. (1998). A helix propensity scale based on experimental studies of peptides and proteins. *Biophys. J.* **75**, 422-427.
84. Skehel, J. J. & Wiley, D. C. (1998). Coiled coils in both intracellular vesicle and viral membrane fusion. *Cell,* **95**, 871-874.
85. Dubay, J. W., Roberts, S. J., Brody, B. & Hunter, E. (1992). Mutations in the leucine zipper of the human immunodeficiency virus type 1 transmembrane glycoprotein affect fusion and infectivity. *J. Virol.* **66**, 4748-4756.
86. Lu, M., Ji, H. & Shen, S. (1999). Subdomain folding and biological activity of the core structure from human immunodeficiency virus type 1 gp41: implications for viral membrane fusion. *J. Virol.* **73**, 4433-4438.
87. Kunkel, T. A., Roberts, J. D. & Zakour, R. A. (1987). Rapid and efficient site-specific mutagenesis without phenotypic selection. *Methods Enzymol.* **154**, 367-382.
88. Sambrook, J., Fritsch, E. F. & Maniatis, T. (1989). *Molecular Cloning: A Laboratory Manual*, Cold Spring Harbor Laboratory Press, Cold Spring Harbor, NY.
89. Studier, F. W., Rosenberg, A. H., Dunn, J. J. & Dubendorff, J. W. (1990). Use of T7 RNA polymerase to direct expression of cloned genes. *Methods Enzymol.* **185**, 60-89.
90. Edelhoch, H. (1967). Spectroscopic determination of tryptophan and tyrosine in proteins. *Biochemistry,* **6**, 1948-1954.
91. Shu, W., Ji, H. & Lu, M. (1999). Trimerization specificity in HIV-1 gp41: analysis with a GCN4 leucine zipper model. *Biochemistry,* **38**, 5378-5385.
92. Johnson, M. L., Correia, J. J., Yphantis, D. A. & Halvorson, H. R. (1981). Analysis of data from the analytical ultracentrifuge by nonlinear least-squares techniques. *Biophys. J.* **36**, 575-588.
93. Laue, T. M., Shah, B. D., Ridgeway, T. M. & Pelletier, S. L. (1992). Computer-aided interpretation of analytical sedimentation data for proteins. In *Analytical Ultracentrifugation in Biochemistry and Polymer Science* (Harding, S. E., Rowe, A. J. & Horton, J. C., eds), pp. 90-125, Royal Society of Chemistry, Cambridge.
94. Plotnikov, V. V., Brandts, J. M., Lin, L. N. & Brandts, J. F. (1997). A new ultrasensitive scanning calorimeter. *Anal. Biochem.* **250**, 237-244.
95. Kraulis, P. (1991). MOLSCRIPT: a program to produce both detailed and schematic plots of protein structures. *J. Appl. Crystallog.* **24**, 924-950.
96. Marky, L. A. & Breslauer, K. J. (1987). Calculating thermodynamic data for transitions of any molecularity from equilibrium melting curves. *Biopolymers,* **26**, 1601-1620.

Appendix

Analysis of CD data

Analysis of heat and denaturant-induced unfolding curves followed the formalism describing a simple two-state conformational transition between folded trimer, T, and unfolded random-coil monomer, M. At each temperature or denaturant concentration, the observed molar ellipticity per residue, [θ], equals:

$$[\theta] = f_M[\theta_M] + (1 - f_M)[\theta_T] \quad \text{(A1)}$$

where f_M is the fraction of monomeric peptide and $[\theta_M]$ and $[\theta_T]$ are the molar ellipticity per residue of M and T, respectively. $[\theta_M]$ and $[\theta_T]$ were assumed to be linear functions of temperature or denaturant concentration of the general form $[\theta_i] = [\theta_{i,0}] + \alpha_i T$ or $[\theta_i] = [\theta_{i,0}] + \alpha_i$[denaturant], with i indicating the M or T state. For a given total concentration of trimer, C_{tot}, the equilibrium unfolding constant, K_{unf}, is expressed by:

$$K_{unf} = \frac{27 f_M^3 C_{tot}^2}{1 - f_M} \quad \text{(A2)}$$

f_M is calculated from the only real solution of this equation:

$$f_M = \sqrt[3]{k\left(\frac{1}{2} + \frac{\sqrt{3}\sqrt{4k+27}}{18}\right)} - \frac{1}{3}\frac{k}{\sqrt[3]{k\left(\frac{1}{2} + \frac{\sqrt{3}\sqrt{4k+27}}{18}\right)}} \quad \text{(A3)}$$

where:

$$k = \frac{K_{unf}}{27 C_{tot}^2}$$

The unfolding enthalpy at the transition midpoint T_m ($f_M = 0.5$), ΔH_m, can be obtained from the temperature-dependence of K_{unf} according to:

$$K_{unf}(T) = \frac{27 f_M 3 C_{tot}^2}{1 - f_M} \exp\left\{\frac{\Delta H_m}{R}\left(\frac{1}{T_m} - \frac{1}{T}\right) - \frac{\Delta C_p}{RT}\left[T - T_m - T\ln\left(\frac{T}{T_m}\right)\right]\right\} \quad \text{(A4)}$$

R is the gas constant and ΔC_p is the heat capacity change. Equations (A1)-(A4) can be combined to analyze thermal unfolding curves by non-linear curve optimization. In principle, the fitting yields ΔH_m, T_m, ΔC_p, $[\theta_{i,0}]$ and α_i. In practice, ΔH_m, T_m and ΔC_p are strongly interdependent and the statistical significance of fitting values extracted by analysis of a single trace is low. However, when ΔC_p is small as compared to ΔH_m, the second term in the curly brackets of equation (A4) is small and can be neglected in the fitting. ΔC_p was obtained from a plot of ΔH_m *versus* T_m.

In a different treatment, $[\theta_M]$ and $[\theta_D]$ were defined by linear regression from the linear pre-transitional and post-transitional parts of the CD trace to obtain a plot of $f_M = ([\theta] - [\theta_T])/([\theta_M] - [\theta_T])$ against T. From such plots, ΔH_m was calculated as:[96]

$$\Delta H_m = 8RT_m^2\left(\frac{\partial f_M}{\partial T}\right)_{T=T_m} \quad \text{(A5)}$$

Results obtained by the two methods were identical within error.

Once ΔH_m, T_m and ΔC_p are known, the unfolding free energy change, ΔG_{unf}, is calculated with help of the Gibbs-Helmholtz equation adapted to monomer-trimer equilibrium:

$$\Delta G_{unf}(T) = -RT\ln K_{unf}(T) = \Delta H_m\left(1 - \frac{T}{T_m}\right) + \Delta C_p\left[T - T_m - T\ln\left(\frac{T}{T_m}\right)\right] - RT\ln K_{unf}(T_m) \quad \text{(A6)}$$

$K_{unf}(T_m) = 27 f_M^3 C_{tot}^2/(1 - f_M) = 6.75 C_{tot}^2$ in the case of a homotrimeric systems.

Molar ellipticity changes observed in isothermal denaturant titrations were treated according to the linear extrapolation model (LEM) in two ways. (i) The experimental data were first transformed to plots of $f_M = ([\theta] - [\theta_T])/([\theta_M] - [\theta_T])$ against denaturant concentration [D]. K_{unf}(D) at each [D] was calculated according to equation (A2). The free energy of unfolding in the presence of denaturants, ΔG(D), is given by:

$$\Delta G(D) = -RT\ln K_{unf}(D) = \Delta G(W) - m_D[D] \quad \text{(A7a)}$$

where m_D in units of kJ mol^{-1} M^{-1} describes the linear dependence of ΔG(D) on [D]. ΔG(W) was calculated from equation (A7) by extrapolation of ΔG(D) to zero denaturant concentration using the data around $[D]_{1/2}$, the denaturant concentration where the unfolding transition is half completed. (ii) Equations (A1)-(A3) and (A7) can be combined to obtain a fitting function suitable to perform a non-linear regression analysis of the unprocessed experimental data resulting in optimized values for ΔG(W), m_D, $[\theta_{M,0}]$, α_M, $[\theta_{T,0}]$ and α_T. In practice, faster convergence and higher statistical significance of the fitting procedure was achieved by using $[D]_{1/2}$ instead of ΔG(W) as a floating parameter. Since $k = f_M^3/(1 - f_M)$, $K_{unf}/27C_{tot}^2 = 0.25$ for $f_M = 0.5$ at $[D] = [D]_{1/2}$. Re-writting equation (A7) by substitution of [D] by $[D]_{1/2}$ yields:

$$\Delta G(\mathrm{W}) = m_{\mathrm{D}}[\mathrm{D}]_{1/2} + \Delta G(\mathrm{D}_{1/2})$$
$$= m_{\mathrm{D}}[\mathrm{D}]_{1/2} - RT\ln\frac{27C_{\mathrm{tot}}^2}{4} \quad \text{(A7b)}$$

Combination of equations (A1)-(A3) and (A7a) and (A7b) results in the following expression, which relates the observed changes in ellipticity to the denaturant concentration:

$$[\theta] = [\theta_{\mathrm{T},0}] + \alpha_{\mathrm{T}}[\mathrm{D}] + ([\theta_{\mathrm{M},0}] + \alpha_{\mathrm{M}}[\mathrm{D}] - [\theta_{\mathrm{T},0}] - \alpha_{\mathrm{T}}[\mathrm{D}])$$
$$\times\left(-\frac{a}{b\sqrt[3]{\frac{a}{c}+\frac{ad}{e}}} + \sqrt[3]{\frac{a}{c}+\frac{ad}{e}}\right) \quad \text{(A8)}$$

where:

$$a = \exp\left\{\frac{-m_{\mathrm{D}}[\mathrm{D}] + m_{\mathrm{D}}\left([\mathrm{D}]_{1/2} + \frac{RT\ln(27C_{\mathrm{tot}}^2/4)}{m_{\mathrm{D}}}\right)}{RT}\right\}$$

$$b = 81C_{\mathrm{tot}}^2$$

$$c = 54C_{\mathrm{tot}}^2$$

$$d = \sqrt{27 + \frac{4a}{27C_{\mathrm{tot}}^2}}$$

$$e = 162\sqrt{3}C_{\mathrm{tot}}^2$$

Once $[\mathrm{D}]_{1/2}$ and m_{D} are known, the free energy of unfolding in water is calculated by:

$$\Delta G(\mathrm{W}) = m_{\mathrm{D}}[\mathrm{D}]_{1/2} - RT\ln\frac{27C_{\mathrm{tot}}^2}{4} \quad \text{(A9)}$$

Analysis of DSC data

The unfolding enthalpy was calculated in three ways. (i) The calorimetric, model-independent enthalpy, $\Delta H(\mathrm{cal})$, was obtained by integration of the excess heat capacity function, $\langle C_{\mathrm{p}}\rangle^{\mathrm{ex}}$, above the baseline defined by the intrinsic change in heat capacity, $\langle C_{\mathrm{p}}\rangle^{\mathrm{int}}$. This latter function was constructed by extrapolation of the pre and post-transitional linear portions of the heat capacity function in proportion to the progress of heat absorption. Generally, for unfolding reactions of molecularity higher than 1, the temperature of maximal heat absorption does not coincide with the temperature at which the system is half-unfolded.[1,2] Since the difference between the heat capacities of the folded and unfolded states in the transition zone was much smaller than $\langle C_{\mathrm{p}}\rangle_{\max}$, the exact definition of the ''progress'' baseline did not introduce a noticeable error in $\Delta H(\mathrm{cal})$. (ii) The effective van't Hoff enthalpy, $\Delta H(\mathrm{vH})$, was calculated according to Privalov & Potekhin:[2]

$$\Delta H(\mathrm{vH}) = (\sqrt{n}+1)T_{\mathrm{m}}\sqrt{R\left[\langle C_{\mathrm{p}}\rangle_{\max} - \frac{\Delta C_{\mathrm{p}}\sqrt{n}}{(\sqrt{n}+1)}\right]} \quad \text{(A10)}$$

$n = 3$ for a trimolecular transition. (iii) The validity of the two-state model of unfolding accompanied by subunit dissociation was tested by non-linear regression analysis of $\langle C_{\mathrm{p}}\rangle^{\mathrm{ex}}$ according to the following equation:

$$\langle C_{\mathrm{p}}\rangle = \langle C_{\mathrm{p}}\rangle^{\mathrm{int}} + \langle C_{\mathrm{p}}\rangle^{\mathrm{ex}}$$
$$= \langle C_{\mathrm{p}}\rangle^{\mathrm{int}} + \frac{\Delta H^2}{RT^2}\left[\frac{f_{\mathrm{M}}(1-f_{\mathrm{M}})}{n - f_{\mathrm{M}}(n-1)}\right] \quad \text{(A11)}$$

n is the number of peptide chains and f_{M} can be solved numerically from:

$$K_{\mathrm{unf}} = \frac{f_{\mathrm{M}}^n n^n C_{\mathrm{tot}}^{n-1}}{1-f_{\mathrm{M}}} \quad \text{(A12)}$$

where C_{tot} is the total concentration of n-mers and $K_{\mathrm{unf}}(T)$ is calculated with reference to $T_{\mathrm{m0.5}}$ ($f_{\mathrm{M}} = 0.5$) by:

$$K_{\mathrm{unf}}(T) = 0.5^{n-1} n^n C_{\mathrm{tot}}^{n-1} \exp\left[-\frac{\Delta H}{RT}\left(1 - \frac{T}{T_{\mathrm{m0.5}}}\right)\right.$$
$$\left. - \frac{\Delta C_{\mathrm{p}}}{RT}\left(T - T_{\mathrm{m0.5}} - T\ln\frac{T}{T_{\mathrm{m0.5}}}\right)\right] \quad \text{(A13)}$$

Fits were also performed according to a formalism with explicit specification of the stoichiometry of unfolding transition:

$$\langle C_{\mathrm{p}}\rangle = \langle C_{\mathrm{p}}\rangle^{\mathrm{int}} + \langle C_{\mathrm{p}}\rangle^{\mathrm{ex}} = f_{\mathrm{M}}C_{\mathrm{p,M}} + (1-f_{\mathrm{M}})C_{\mathrm{p,T}}$$
$$+ \frac{\Delta H^2}{RT^2}\left[\frac{f_{\mathrm{M}}(1-f_{\mathrm{M}})}{3-2f_{\mathrm{M}}}\right] \quad \text{(A14)}$$

where $\Delta H = \Delta H_{\mathrm{m0.5}} + \Delta C_{\mathrm{p}}(T - T_{\mathrm{m0.5}})$. $C_{\mathrm{p,M}}$ and $C_{\mathrm{p,T}}$ are the heat capacities of the monomeric unfolded state and the trimeric folded state, respectively, and f_{M} is calculated by equation (A3). Results obtained by application of the combined equations (A11)-(A13); n was a floating parameter) or by the combined equations (A2), (A3), and (A14) were the same.

Error analysis

Errors in thermodynamic functions derived from fitted parameters were estimated from the variance. The variances in $\Delta H_{\mathrm{unf}}(T)$ and $\Delta G_{\mathrm{unf}}(T)$ are given, respectively, by:

$$\sigma_{\Delta H} = \sigma_{\Delta H\mathrm{m}}^2 + \sigma_{\Delta C\mathrm{p}}^2(T - T_{\mathrm{m}})^2 + \sigma_{T\mathrm{m}}^2\Delta C_{\mathrm{p}}^2 \quad \text{(A15a)}$$

and:

$$\sigma_{\Delta G} = \sigma^2_{\Delta Hm}(1 - T/T_m)^2 + \sigma^2_{\Delta Cp}[(T - T_m - T\ln(T/T_m)]^2 + \sigma^2_{Tm}[\Delta C_p(T/T_m - 1) + \Delta H_m T/T_m^2]^2 + \sigma^2_{Ctot}(RT/C_{tot})^2 \quad \text{(A15b)}$$

The error of ΔH_m ($\sigma_{\Delta Hm}$) from CD experiments was estimated as follows. For each individual melting curve, ΔH_m was calculated according to equations (A1)-(A5) with the slopes of the pre-transition baseline, or post-transition baseline, or both at the same time, being either free-floating or fixed parameters. Since there was no statistically significant trend for the slopes to vary with mutation and peptide concentration, the slopes were fixed either as the mean slope of the entire data set or the mean slope observed for each protein. This procedure resulted in six to ten values of ΔH_m, from which a standard deviation of kJ mol^{-1} (5-10 % of the mean, depending on the mean ΔH_m) was calculated. Linear fit of ΔH_m *versus* T_m (Figure 9 of the main text) resulted in a fitting error of ΔC_p of the order of 0.8 kJ K^{-1} mol^{-1}, except for N34(L6)C28, for which the error was 2 kJ K^{-1} mol^{-1}. A more reliable estimate of $\sigma_{\Delta Cp}$, 1.7-2 kJ K^{-1} mol^{-1} (20 %), was obtained by systematic truncation of the data by one point at a time. The terms including errors in T_m and C_{tot} could be neglected, since the error in T_m was <1 K and the error in C_{tot} was <10 %. According to equations (A15a) and (A15b) and using $\sigma_{\Delta Cp}$ and $\sigma_{\Delta Hm}$ obtained as explained above, the maximal errors in $\Delta H_{unf}(T)$ and $\Delta G_{unf}(T)$ were 45-60 kJ mol^{-1} (10-12 %) and 1.6-3.2 kJ mol^{-1} (1-6 %), respectively, for the extrapolation away from T_m to 62 °C. Maximal errors in $\Delta\Delta H_{unf}(T)$ and $\Delta\Delta G_{unf}(T)$ were, therefore, 70 kJ mol^{-1} and 5 kJ mol^{-1}, respectively. Values of $T\Delta S_{unf}(T)$ and $T\Delta\Delta S_{unf}(T)$, calculated from ΔH_{unf} and ΔG_{unf} contained the same uncertainty.

The errors in m_D and ΔG(W) were estimated comparing the results obtained from of equation (A7) by using varying number of points around $[D]_{1/2}$ for extrapolation to zero denaturant concentration. Maximum error of m_D was 1 kJ mol^{-1} M^{-1} and maximum error of ΔG(W) was 5 kJ mol^{-1}.

References

1. Freire, E. (1989). Statistical thermodynamic analysis of the heat capacity function associated with protein folding-unfolding transitions. *Comm. Mol. Cell. Biophys.* **6**, 123-140.

2. Privalov, P. L. & Potekhin, S. A. (1986). Scanning microcalorimetry in styding temperature-induced changes in proteins. *Methods Enzymol.* **131**, 4-51.

Edited by I. B. Holland

(Received 4 October 2000; received in revised form 10 January 2001; accepted 15 January 2001)